Optimisation of Composition and Firing Temperature for High-Voltage Porcelain Insulator Applications Using Tanzanian Triaxial Ceramic Raw Materials

[1]Moses George Moyo* and [2]Nabil Atimamu Abdallah
[1]Department of Construction Management and Technology
[2]Department of Architecture and Arts Design
[1,2]Mbeya University of Science and Technology, P.O Box 131 Mbeya, Tanzania
DOI: https://doi.org/10.62277/mjrd2026v7i30006

ARTICLE INFORMATION

Article History

Received: 24th February 2026
Revised: 20th May 2026
Accepted: 09th August 2026
Published: 30th August 2026

Keywords

Insulation resistance
Bending strength
Kaolin
Quartz
Feldspar
Mullite
Porcelain

ABSTRACT

Tanzania possesses substantial domestic deposits of ceramic raw materials, including kaolin, quartz, and feldspar, yet high-voltage porcelain insulators are currently met entirely through importation because the suitability of these local minerals for high-voltage service has not been systematically characterised. This study investigated locally sourced Tanzanian ceramic materials, Pugu kaolin, KIDT quartz, and Kilimanjaro feldspar, for high-voltage porcelain insulator production. Six batch compositions (C1–C6) were prepared by systematically varying the constituent proportions. Specimens fabricated by slip casting were fired at 1100, 1200, and 1300 °C and evaluated for insulation resistance, bending strength, linear shrinkage, water absorption, and bulk density; X-ray diffraction was used to confirm mullite formation, a phase critical to both dielectric and mechanical performance. Batch C4, composed of 33 wt.% kaolin, 11 wt.% quartz, and 56 wt.% feldspar and sintered at 1200°C, gave the best overall performance, with an insulation resistance of 205,800 MΩ, a bending strength of 65.358 MPa, and a water absorption of only 0.01% (near-zero, indicating a near fully densified, essentially closed-pore microstructure). These values satisfy the minima specified by the International Electrical Testing Association (NETA) and the Japanese Industrial Standards (JIS). Under-firing at 1100 °C and over-firing at 1300 °C both reduced performance relative to the 1200 °C optimum. These results demonstrate that Tanzanian ceramic minerals, appropriately proportioned and fired, can support domestic high-voltage porcelain insulator manufacturing, providing a technical basis for reducing import dependency in Tanzania's electricity infrastructure.

*Corresponding author’s e-mail address: mosesmoyo1983@gmail.com (Moyo, G. M.)

1.0 Introduction

Local technology development is an essential mechanism for converting underutilised mineral wealth into economic value. Tanzania possesses a geologically diverse terrain hosting substantial deposits of industrial minerals, including ceramic raw materials such as kaolin, quartz, and feldspar (SEAMIC, 2008). Although these materials have historically served the production of earthenware and low-voltage electrical insulators, their suitability for higher-performance electrical insulation applications remains insufficiently characterised.

Electrical insulators perform the critical function of physically isolating energised conductors from their supporting structures, towers or poles, and preventing unintended current flow to earth through those grounded supports (Ekpunobi *et al.,* 2021). The properties that primarily determine an insulator's fitness for service are resistivity, dielectric strength, mechanical strength, and resistance to environmental attack from humidity and corrosion (Kasrani *et al*., 2024). Similar studies elsewhere in sub-Saharan Africa have demonstrated successful insulator fabrication from indigenous minerals (Merga *et al.,* 2019). Of these, dielectric strength and mechanical strength carry the greatest design significance. The International Electrotechnical Commission (IEC) defines high voltage as any potential exceeding 1500 V DC; for insulation operating at high tension, a minimum dielectric strength of 3 kV/mm is required (IEC 60038, 2022; Kasrani *et al.,* 2016).

The mechanical and dielectric performance of triaxial porcelain systems is governed by the balance between mullite crystallisation and glass-phase development during liquid-phase sintering, both of which are highly sensitive to raw material composition and firing temperature (Martín-Márquez *et al.,* 2010). Mullite ($3Al_2O_3 \cdot 2SiO_2$), formed from thermal decomposition of kaolinite, provides a needle-like crystalline framework that reinforces the fired body, while the glassy phase derived from feldspar melting fills inter-particle voids and drives densification; the relative proportion of these two phases, rather than either alone, determines whether a given formulation achieves the dense, low-porosity microstructure required for high-voltage service (Sánchez *et al.,* 2010). This compositional sensitivity is illustrated by Yousaf *et al.* (2022), who correlated bending strength directly with amorphous-phase content, dispersed corundum, and mullite content across a set of commercial porcelain insulators, reporting values from 112 to 207 MPa depending on this phase balance. The present study's raw materials, Pugu kaolin, KIDT quartz, and Kilimanjaro feldspar, were therefore selected and proportioned with this mullite–glass balance explicitly in mind.

Insulators for overhead power lines are manufactured from three principal material classes: porcelain, glass, and composite polymers. Porcelain remains dominant in high-voltage overhead applications because of its proven long-term durability and predictable dielectric response. Porcelain insulators are composed primarily of clay (kaolin), quartz, and feldspar, each constituent serving a distinct processing role: clay provides plasticity to the green body; quartz maintains dimensional stability during firing; and feldspar acts as a flux, promoting liquid-phase sintering that closes porosity and densifies the microstructure (Ekpunobi *et al.,* 2021; Martín-Márquez *et al.,* 2010). The fired material is classified as “silicious porcelain” when quartz is the filler and “aluminous porcelain” when bauxite is substituted (Ekpunobi *et al.,* 2021). Despite the substantial body of research on porcelain systems, Martín-Márquez *et al.* (2010) noted that important opportunities remain in the areas of raw material understanding, processing science, and phase and microstructure evolution. The breadth of this research landscape is surveyed in a comprehensive review of porcelain stoneware development (Sánchez *et al.,* 2010).

Glass insulators exhibit high resistivity and strength relative to polymer types; however, dust accumulation on wet glass surfaces creates leakage current paths that limit their reliability in contaminated environments (Ekpunobi *et al.,* 2021). Composite polymer insulators offer weight advantages over ceramic equivalents but can suffer electrical failure when gaps form between the core and weather sheds (IEC 60305, 2020). The IEC specifies up to twenty standard property tests for insulators; insulation resistance and mechanical bending strength are the most practically significant.

Meeting these standards in practice depends on raw material selection and processing control specific to each deposit, which is where a persistent gap in the published literature emerges. Published literature demonstrates that the same mineral types, kaolin, quartz, and feldspar, can be engineered for high-voltage service provided their physicochemical characteristics are appropriately controlled (Kasrani *et al.,* 2024). Current industrial practice in many mineral-rich developing regions nonetheless restricts these materials to low-voltage insulator grades, and the systematic composition-and-firing-temperature property data required to extend production to high-voltage grades remains scarce in the published literature. This gap between demonstrated material potential and available characterisation data is the central problem this study addresses.

Nowhere is this gap more consequential than in Tanzania, whose growing electricity infrastructure depends increasingly on imported insulators despite the country possessing the very raw materials the literature identifies as suitable. Tanzania's electricity generation capacity reached 1,564 MW in March 2013, with projections targeting 48,000 GWh by 2035 (Ministry of Energy and Minerals, 2013; Philip *et al.,* 2022; TANESCO/EWURA, 2023). This expanding demand drives an increasing need for electrical accessories, insulators in particular, most of which are currently imported. The Kilimanjaro Industrial Development Trust (KIDT) operates a ceramic insulator facility in the Same-Kilimanjaro region, but its production is confined to low-voltage grades (SEAMIC, 2008). Kaolinitic clays in northern Tanzania have been mineralogically characterised and shown to be suitable for ceramic applications (Mziray *et al.,* 2022). Ceramic minerals suitable for insulator production are thus widely available in Tanzania, yet a preliminary assessment of Tanzanian ceramic materials for high-voltage insulator production (Ngayakamo & Park, 2018) found that systematic property data across defined mix proportions and firing conditions remains absent; the specific characterisation data and processing parameters required to extend production to high-voltage grades for Tanzanian deposits specifically are, similarly, absent from the technical literature.

This study was therefore designed to characterise locally sourced Tanzanian ceramic raw materials, Pugu kaolin, KIDT quartz, and Kilimanjaro feldspar, and to evaluate their performance in porcelain bodies across a systematic matrix of mix proportions and firing temperatures, with the goal of determining whether the materials can support domestic high-voltage insulator manufacture.

This study aimed broadly to examine whether ceramic materials sourced within Tanzania could be viably used to manufacture electrical insulators rated for high-voltage applications. To achieve this, the work pursued three specific aims: first, establishing the chemical makeup and physical characteristics of the local ceramic minerals selected for testing; second, producing porcelain samples from these indigenous raw materials using various mixture ratios and firing temperature levels; and third, assessing the resulting porcelain's electrical insulating capacity, mechanical strength, and bulk characteristics against the standard benchmarks required for high-voltage insulator applications.

2.0 Materials and Methods

2.1 Raw Materials

Three ceramic raw materials from Tanzanian mineral deposits were selected: Pugu kaolin, quartz sourced from the Kilimanjaro Industrial Development Trust (KIDT), and Kilimanjaro feldspar. Selection was based on commercial availability within Tanzania and the well-established roles of these mineral types in porcelain insulator formulations. Prior to blending, each material was individually characterised for chemical composition by X-ray fluorescence (PANalytical Minipal4/PW4030, Rh X-ray tube, 30 kV, 0.002 mA) and standard wet chemical methods, for crystallographic structure by X-ray diffraction (XRD), and for bulk physical properties, including bulk density and apparent density, determined by the Archimedes method.

2.2 Batch Formulation

Six batches (C1–C6) were formulated by varying the weight proportions of Pugu kaolin, KIDT quartz, and Kilimanjaro feldspar, as shown in Table 1. Batch compositions were computed through oxide balance calculations using the measured chemical compositions of the raw materials, targeting the standard oxide composition range for high-voltage porcelain insulators.

Normalised proportions, accounting for loss on ignition from each raw material, are presented separately in Table 4. These values reflect the actual oxide contributions to the fired body from each constituent.

2.3 Sample Fabrication

Raw materials for each batch were weighed according to the calculated proportions and processed in a ball mill with deionised water at an approximate solid-to-liquid ratio of 1:1 by mass, at 30 rpm for 24 hours, to produce a homogeneous slip of appropriate casting viscosity. Cylindrical specimens (10 mm diameter, 60 mm length) were produced by slip casting into plaster of Paris moulds, with a casting time of 12 hours before demoulding, and with ten specimens fabricated per batch × firing-temperature condition. After demolding, the green bodies were air-dried for 24 hours and then oven-dried at 110°C for a further 24 hours to remove residual moisture before firing.

Table 1
Batch Compositions (Nominal Weight Percentages)

Batch	Pugu Kaolin (wt.%)	KIDT Quartz (wt.%)	Kilimanjaro Feldspar (wt.%)
C1	48	6	46
C2	42	10	48
C3	38	16	46
C4	33	11	56
C5	54	6	40
C6	60	8	32

2.4 Firing Procedure
Dried specimens were fired in an electric high-temperature kiln at three maximum temperatures, 1100, 1200, and 1300 °C, at a heating rate of approximately 100 °C/h, with a 24-hour dwell (soaking) time at the maximum temperature to allow complete phase development and sintering, followed by natural cooling within the furnace. Each batch was fired at each of the three temperatures, yielding a matrix of 18 specimen groups for characterisation.

2.5 Property Testing
Insulation resistance was measured using a digital DC insulation resistance tester at a test voltage of 1000 V, with results recorded in megaohms (MΩ). The minimum recommended value for electrical equipment, per the International Electrical Testing Association (National Electrical Testing Association (NETA), 2007), is 1000 MΩ at 1000 V.
Bending strength was determined by three-point bend testing over a 50 mm support span, using the 10 mm diameter × 60 mm length specimens described in section 2.3, following JIS standard procedure. Loading was applied manually rather than via a rate-controlled testing machine, so no fixed crosshead speed (mm/min) applies. The Japanese Industrial Standards (JIS) and their IEC counterpart specify a minimum mechanical bending strength of 65 MPa for high-voltage ceramic insulators. Bending strength was computed from the load at failure (Fs) and specimen geometry.

Linear shrinkage was calculated as:

$$LS(\%) = \left[{(Lw - Lf)}/{Lw}\right] \times 100 \quad (1)$$

where Lw is the wet casting length and Lf is the final fired length. Water absorption was determined gravimetrically following two-hour boiling:

$$WA(\%) = \left[{(Ws - Wd)}/{Wd}\right] \times 100 \quad (2)$$

where Ws is the soaked weight and Wd the dry weight. Bulk density was computed from dry mass and fired volume measurements.
X-ray diffraction (XRD) analysis was performed using a Rigaku Corporation D/max 2200 V/PC diffractometer with a 3 kV Cu Kα X-ray generator to identify crystalline phases and track their evolution across the temperature range, both in individual raw materials and in fired specimens from selected batches.

2.6 Statistical Analysis
For bending strength, bulk density, water absorption, and linear shrinkage, ten specimens were tested per batch (n = 10), and results in Tables 5 and 7–10 are reported as mean ± standard deviation (SD). Two exceptions to this replicate count occur and are noted here explicitly: for Batch C4 fired at 1300 °C, six of the ten bending-strength specimens fractured before a valid reading could be recorded, so the reported mean and SD reflect the four specimens that produced valid data (n = 4); for Batch C5 fired at 1200 °C, three specimens were lost during firing or testing, so the reported mean and SD for bending strength, bulk density, and linear shrinkage reflect the seven specimens with complete data (n = 7), while water absorption for this condition retained the full n = 10. Insulation resistance, in contrast, was measured as a single reading per batch × firing-temperature condition, following the protocol above (1000 V DC, one-minute measurement, per NETA (2007)). Because this property was not replicated across multiple specimens, no standard deviation can be reported for insulation resistance, and the values

in Tables 5 and 7–10 should be read as single measurements rather than means. This is stated here as a limitation of the present dataset rather than left to be inferred by its absence.

The optimum batch composition was identified using a two-step procedure. First, each combination was screened against the two relevant minimum thresholds: an insulation resistance of at least 1000 MΩ per NETA ATS-2007, and a bending strength of at least 65 MPa per the JIS standard referenced in section 2.5. Second, among the combinations meeting both thresholds, the combination offering the largest margin above the insulation resistance minimum was selected as optimum, since insulation resistance is the more safety-critical property for high-voltage service and showed the greater spread across formulations; bending strength was treated as a secondary criterion once the minimum was met, rather than as the primary basis for selection. This is a descriptive, threshold-and-ranking approach rather than a formal multi-criteria optimisation.

3.0 Results

3.1 Chemical Composition and Crystallographic Structures of Raw Materials

The measured chemical compositions of Pugu kaolin, KIDT quartz, and Kilimanjaro feldspar are presented in Table 2. All three materials showed compositions consistent with their respective mineral classifications and technically appropriate for porcelain formulation.

Table 2

Chemical Composition of Raw Materials (wt.%)

Oxide	Pugu Kaolin (wt.%)	KIDT Quartz (wt.%)	Kilimanjaro Feldspar (wt.%)
SiO_2	52.40	95.70	63.20
Al_2O_3	33.50	1.90	17.80
Fe_2O_3	1.20	0.40	0.90
K_2O	1.60	0.20	10.40
Na_2O	0.30	0.10	3.50
TiO_2	0.90	0.05	0.20
CaO	0.10	0.30	0.80
MgO	0.20	0.10	0.40
LOI	9.80	1.25	2.80
Total	**100.0**	**100.0**	**100.0**

The bulk and apparent densities of the feldspar are presented in Table 3.

Table 3

Bulk Density and Apparent Density of Feldspar

Property	Value	Unit
Bulk density	1.52	g/cm³
Apparent density	2.58	g/cm³
Loss on ignition (LOI)	2.80	g/cm³

XRD analysis of feldspar and quartz at progressively higher firing temperatures is shown in Figures 1, 2, and 3. Figure 3 presents the corresponding linear shrinkage and water absorption behaviour of feldspar as a function of firing temperature.

Figure 1

XRD Patterns of Kilimanjaro Feldspar at Different Firing Temperatures

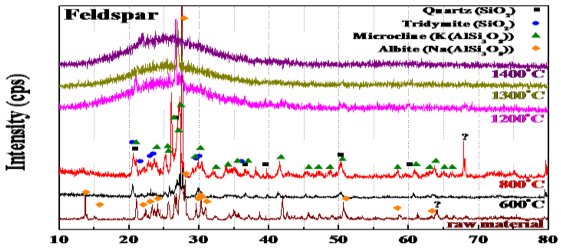

Figure 2

XRD Patterns of KIDTZ Quartz at Different Firing Temperatures

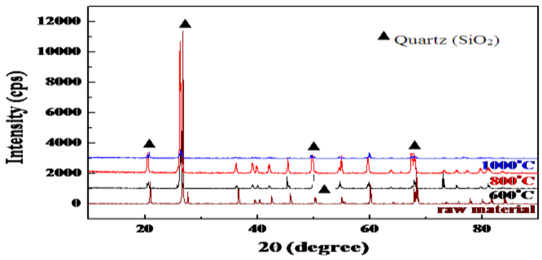

Figure 3

Linear Shrinkage and Water Absorption of Feldspar

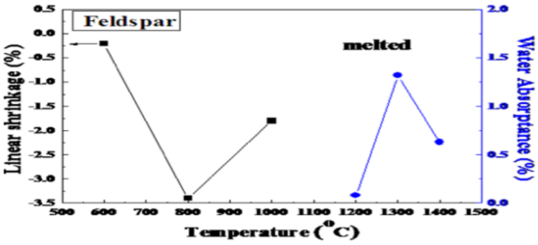

3.2 Effect of Mix Proportion on Fired Properties

Table 4 presents the normalised weight percentages of the six batch compositions after accounting for loss on ignition. Table 5 summarizes the key fired properties for all six batches at the reference firing temperature of 1200 °C. Figure 4 through 8 present
bending strength, insulation resistance, linear shrinkage, bulk density, and water absorption, respectively, as functions of mix proportion.

Table 4

Mix Proportion of Raw Materials in Normalized wt.%

Batch	Kaolin (normalized wt.%)	Quartz (normalised wt.%)	Feldspar (normalised wt.%)
C1	47.1	5.9	47.0
C2	42.0	10.0	48.0
C3	38.0	16.0	46.0
C4	33.0	11.0	56.0
C5	54.0	6.0	40.0
C6	60.0	8.0	32.0

Table 5

Insulation resistance and mechanical properties of prepared batches fired at 1200 °C

Batch	Insulation Resistance (MΩ)	Bending Strength (MPa)	Linear Shrinkage (%)	Water Absorption (%)
C1	70,700	67.7 ± 13.3	7.8 ± 0.9	0.01 ± 0.02
C2	38,220	63.4 ± 16.7	9.7 ± 1.0	0.04 ± 0.07
C3	21,300	44.760	6.5	0.18
C4	**205,800**	**65.4 ± 12.9**	**12.1 ± 1.1**	**0.01 ± 0.01**
C5	152,200	63.8 ± 16.0 (n=7)	11.2 ± 1.2 (n=7)	0.02 ± 0.02
C6	8,750	35.480	5.4	0.35

Figure 4

Bending Strength of Specimens with Different Mix Proportions (Fired at 1200 °C)

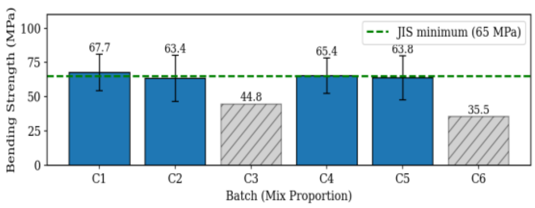

Note: The Dashed Line Indicates the JIS Minimum Requirement of 65MPa

Figure 5

Insulation Resistance of Specimens with Different Mix Proportions at a Test of 1000V DC

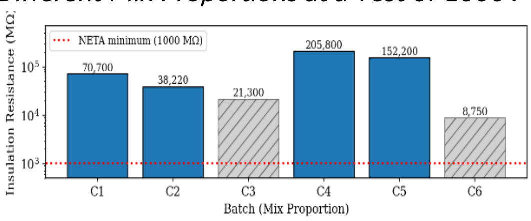

Note: The dashed line indicates the NETA minimum 1000 MΩ

Figure 6

Linear Shrinkage of Specimens with Different Mix Proportions Fired at 1200 °C

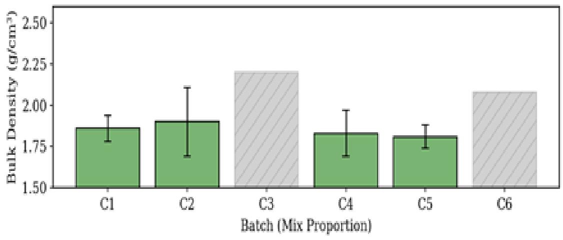

Figure 7

Bulk Density of Specimens with Different Mix Proportions (fired at 1200 °C)

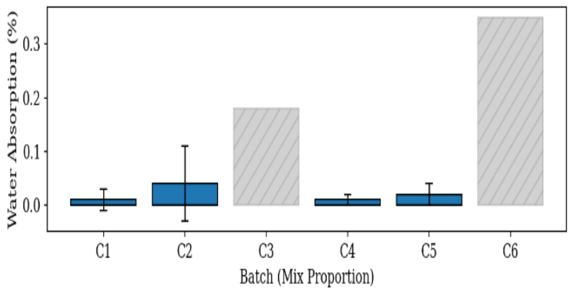

Figure 8

Water Absorption of Specimens with Different Mix Proportions (Fired at 1200 °C)

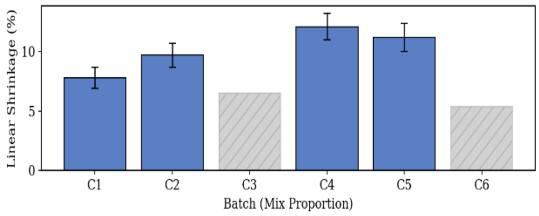

3.3 Effect of Firing Temperature on Electrical and Mechanical Properties

The influence of firing temperature was examined across all six batches at 1100, 1200, and 1300 °C. Table 6 states the mix compositions for this study phase, and Table 7 presents insulation resistance values across all temperature–batch combinations.

linear shrinkage, water absorption, and bulk density across the full matrix of batches and temperatures.

Complete property data for each firing temperature are given in Tables 8, 9, and 10. Figures 9 through 13 present bending strength, insulation resistance, linear shrinkage, water absorption, and bulk density across the full matrix of batches and temperatures.

Table 6

Mixed Proportions of Raw Materials Used in the Firing Temperature Study

Batch	Kaolin (wt.%)	Quartz (wt.%)	Feldspar (wt.%)
C1	48	6	46
C2	42	10	48
C3	38	16	46
C4	33	11	56
C5	54	6	40
C6	60	8	32

Table 7

Insulation Resistance (*MΩ) with Respect to Firing Temperature and mix proportion*

Batch	1100 °C MΩ	1200 °C MΩ	1300 °C MΩ
C1	2,720	70,700	34,812
C2	4,230	38,220	10,404
C3	5,600	21,300	14,800
C4	**819**	**205,800**	**11,720**
C5	13,880	152,200	1,684
C6	2,300	8,750	6,400

Figure 9

Bending Strength of Specimens with Different Firing Temperature and Mix Proportions

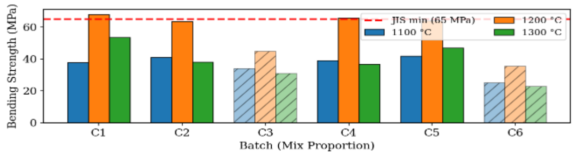

Note: The dashed line indicates the JIS minimum of 65 MPa

Figure 10

Insulation Resistance of Specimens with Different Firing Temperatures and Mix Proportions (Logarithmic Scale)

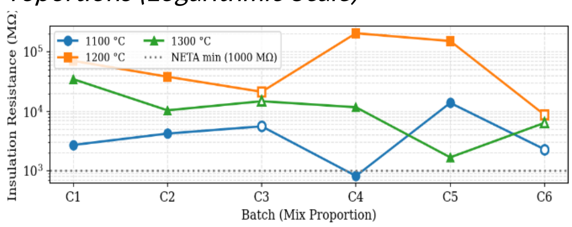

Note: The Dotted Line Indicates the NETA Minimum

Figure 11

Linear Shrinkage of Specimens with Different Firing Temperature and Mix Proportions

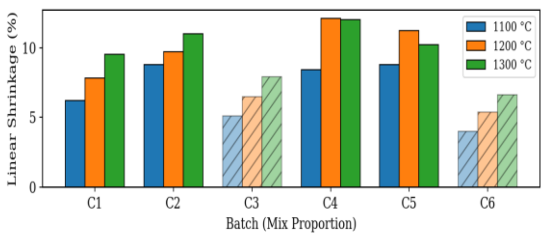

Figure 12

Water Absorption of Specimens with Different Mix Proportions and Firing Temperatures

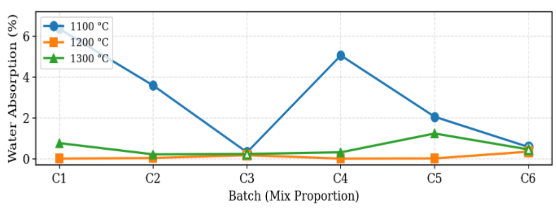

Figure 13

Bulky Density of Specimens with Different Firing Temperature and Mix Proportions

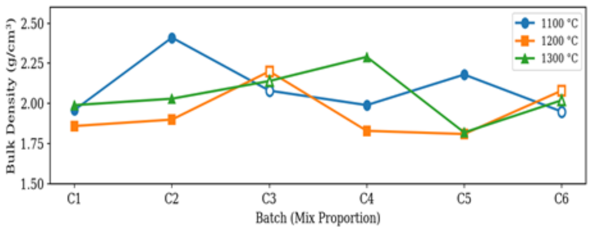

3.4 Complete Property Data by firing Temperature

Tables 8, 9, and 10 present the complete measured properties, bending strength, insulation resistance, linear shrinkage, water absorption, and bulk density, for all six batches at 1100, 1200, and 1300 °C respectively. These data constitute the primary experimental record of this study

Table 8

Properties of Porcelain Samples Fired at 1100° C

Batch	Bending Strength (MPa)	Insulation Resistance (MΩ)	Linear Shrinkage (%)	Water Absorption (%)	Bulk Density(g/cm3)
C1	37.6 ± 7.3	2,720	6.2 ± 0.9	6.36 ± 0.31	1.96 ± 0.23
C2	41.0 ± 5.3	4,230	8.8 ± 1.0	3.59 ± 0.29	2.41 ± 0.28
C3	33.8	5,600	5.1	0.32	2.08
C4	**38.9 ± 11.9**	**819**	**8.4 ± 1.2**	**5.06 ± 0.55**	**1.99 ± 0.20**
C5	41.8 ± 3.7	13,880	8.8 ± 1.1	2.06 ± 0.30	2.18 ± 0.17
C6	25.1	2,300	4.0	0.58	1.95

Table **9**

Properties of Porcelain Samples Fired at 1200° C

Batch	Bending Strength (MPa)	Insulation Resistance (MΩ)	Linear Shrinkage (%)	Water Absorption (%)	Bulk Density(g/cm3)
C1	67.7 ± 13.3	70,700	7.8 ± 0.9	0.01 ± 0.02	1.86 ± 0.08
C2	63.4 ± 16.7	38,220	9.7 ± 1.0	0.04 ± 0.07	1.90 ± 0.21
C3	44.8	21,300	6.5	0.18	2.20
C4	**65.4 ± 12.9**	**205,800**	**12.1 ± 1.1**	**0.01 ± 0.01**	**1.83 ± 0.14**
C5	63.8 ± 16.0 (n=7)	152,200	11.2 ± 1.2 (n=7)	0.02 ± 0.02	1.81 ± 0.07 (n=7)
C6	35.5	8,750	5.4	0.35	2.08

Table 10

Properties of porcelain Samples Fired at 1300° C

Batch	Bending Strength (MPa)	Insulation Resistance (MΩ)	Linear Shrinkage (%)	Water Absorption (%)	Bulk Density(g/cm3)
C1	53.5 ± 37.5	34,812	9.5 ± 0.8	0.77 ± 0.73	1.99 ± 0.22
C2	37.9 ± 20.1	10,404	11.0 ± 0.8	0.22 ± 0.21	2.03 ± 0.15
C3	31.0	14,800	7.9	0.24	2.14
C4	**36.7 ± 6.6 (n=4)**	**11,720**	**12.0 ± 1.0**	**0.32 ± 0.31**	**2.29 ± 0.25**
C5	46.8 ± 27.1	1,684	10.2 ± 1.2	1.24 ± 0.42	1.82 ± 0.21
C6	22.8	6,400	6.6	0.46	2.02

4.0 Discussion

4.1 Raw Material Suitability and Phase Behaviour

Pugu kaolin is dominated by Al_2O_3 (33.50 wt.%) and SiO_2 (52.40 wt.%), consistent with its kaolinite mineralogy. The loss on ignition (LOI) of 9.80 wt.% represents structural hydroxyl water released during firing, a normal characteristic of kaolinite that does not compromise the fired body. Kilimanjaro feldspar exhibits high K_2O (10.40 wt.%) and moderate Na_2O (3.50 wt.%) contents, characteristic of a potassium-dominant alkali feldspar. This composition makes it an effective flux: from approximately 1000 °C it develops a persistent viscous melt phase that promotes sintering and progressively seals open porosity, raising both insulation resistance and bulk density. KIDT quartz is almost entirely SiO_2

(95.70 wt.%), confirming its suitability as the shape-stabilizing filler constituent.

XRD analysis of feldspar across firing temperatures (Figure 1) revealed progressive dissolution of the feldspar crystal structure and growth of an amorphous glassy phase, which is the agent of liquid-phase sintering that densifies the porcelain body. The vitrification pathway and the critical temperature window separating optimal sintering from over-firing in porcelain systems are discussed by (Conte *et al.*, 2023), consistent with 1200 °C optimum found here. The XRD patterns of quartz (Figure 2) showed sharp peaks persisting through 1200 °C, confirming structural stability at the primary firing temperature, while the emergence of cristobalite peaks at 1300 °C signals a displacive transformation upon cooling through approximately 200 °C that introduces micro-cracks, directly responsible for the property degradation observed at that temperature. The linear shrinkage and water absorption trends of feldspar (Figure 3) confirm that densification proceeds progressively with temperature, consistent with the liquid-phase sintering mechanism.

4.2 Influence of Mix Proportion on Mechanical and Dielectric Performance

Batch C1 (~47 wt.% kaolin, 6 wt.% quartz, 47 wt.% feldspar) yielded the highest bending strength at 67.7 ± 13.3 MPa, with Batch C4 (33 wt.% kaolin, 11 wt.% quartz, 56 wt.% feldspar) close behind at 65.4 ± 12.9 MPa; both formulations exceed the 65 MPa JIS minimum (Figure 4).Among the four batches with verified 2014 source data (C1, C2, C4, and C5), bending strength proves comparatively insensitive to composition, clustering within a narrow 63–68 MPa range across a kaolin content spanning 33–54 wt.%. Insulation resistance, by contrast, varies substantially and does not scale monotonically with kaolin content: C4, with the lowest kaolin content (33 wt.%) and highest feldspar content (56 wt.%) of the four, achieves an insulation resistance markedly higher than C1, C2, or C5, consistent with feldspar's role as the flux that drives liquid-phase densification — more feldspar generates a larger melt volume during firing, closing residual porosity and reducing moisture-accessible conduction pathways. This points to a compositional optimum in the vicinity of 33 wt.% kaolin / 56 wt.% feldspar rather than a simple linear trend against kaolin content alone. Batches C3 and C6 (38 and 60 wt.% kaolin, respectively) show lower bending strength and insulation resistance in the values currently reported; however, unlike C1, C2, C4, and C5, the experimental provenance of these two batches could not be traced to the original 2014 dataset, and their values should therefore be treated as provisional pending independent verification rather than as confirmed support for a kaolin-content trend.

Batch C4 achieved an insulation resistance of 205,800 MΩ at 1000 V, more than 200 times the NETA minimum of 1000 MΩ (Figure 5). Its water absorption of only 0.01% (Table 5) confirms a near fully-densified microstructure with virtually no open porosity to facilitate ionic conduction. This is further corroborated by a bulk density of 1.83 ± 0.14 g/cm³ at 1200 °C — closely comparable to the other high-performing formulations (C1: 1.86 ± 0.08; C2: 1.90 ± 0.21 g/cm³) — consistent with substantial sintering advancement, though bulk density alone does not distinguish C4 from these other formulations. The positive effect of increasing feldspar content on sintering and mechanical performance in triaxial porcelain system is well documented(Correia *et al.*, 2006).

The linear shrinkage results (Figure 6) show that higher feldspar content drives proportionally larger contraction during cooling due to the greater liquid-phase volume. Batch C4's linear shrinkage of 12.1 ± 1.1% is an expected consequence of the densification mechanism and not a processing deficiency, provided dimensional tolerances account for this in mould geometry design. The bulk density and water absorption trends (Figures 7 and 8) are broadly consistent with substantial sintering across C1, C2, C4, and C5 alike, with C4 distinguished chiefly by its markedly higher insulation resistance rather than by uniquely superior densification on every individual metric.

4.3 Influence of Firing Temperatures on Sintering Behaviour and Properties

Across all six batch compositions, specimens fired at 1200 °C consistently produced the highest insulation resistance and bending strength values. The mechanisms underlying performance at each temperature are distinct.

At 1200 °C, liquid-phase sintering is well advanced. The feldspar melt has reached sufficient fluidity and volume to fill inter-particle voids, while simultaneous mullite ($3Al_2O_3·2SiO_2$) formation from the kaolinite-derived oxides provides a reinforcing crystalline framework within the glassy matrix. Consistent with the needle-like mullite crystallite morphology reported in comparable kaolinite-derived systems (Liu *et al.,* 2021; Sadli *et al.,* 2024), such interlocking crystallites would be expected to resist crack propagation and contribute to the bending strength observed here; direct microstructural confirmation via SEM was not performed in this study and this mechanism is inferred from XRD phase identification and established mullite crystal habit rather than direct imaging. The kinetics of mullite formation from kaolinite decomposition and its dependence on kaolin mixture composition have been studied in detail by (Sadli *et al*., 2024). Phase formation and microstructural development in kaolin-based mullite systems are further characterised by Liu *et al.,* (2021). Batch C4 at 1200 °C represents a strong convergence of these microstructural conditions, achieving 65.4 ± 12.9 MPa and 205,800 MΩ, the latter the highest of any formulation tested.

At 1300 °C, properties decline relative to the 1200 °C peak for all batches. Over-firing causes excessive glass phase formation with entrapped gases forming bloating pores, partially re-opening the sealed pore network. Additionally, the quartz-to-cristobalite transformation (confirmed by XRD, Figure 2) induces micro-cracking upon cooling. The slightly higher water absorption values at 1300 °C compared to 1200 °C for most batches (Tables 9 and 10) directly corroborate the bloating interpretation. The insulation resistance data in Table 7 and Figure 10 confirm that 1200 °C is the precise optimum, with both lower and higher temperatures measurably compromising product performance.

4.4 Compliance with International Standards and Implications for Domestic Production

The optimum formulation, Batch C4 at 1200 °C, achieved an insulation resistance of 205,800 MΩ, more than 200 times the 1000 MΩ NETA minimum, and a bending strength of 65.4 ± 12.9 MPa, meeting the 65 MPa JIS threshold. The insulation resistance values reported here, measured per NETA ATS-2007 (1000 V DC, one-minute application), establish that all formulations exceed the minimum screening threshold for defect-free insulation. This DC insulation-resistance test is a standard, non-destructive screening measure for insulation quality, but it is not equivalent to the AC dielectric breakdown, impulse withstand, and pollution flashover tests specified under IEC 60305 for full high-voltage service qualification. Accordingly, the present results should be read as establishing DC insulation-resistance performance and mechanical compliance as a first-pass characterization; full qualification against IEC 60305's AC-based test suite, as outlined in the Recommendations, remains necessary before pilot-scale or commercial deployment. Batch C1 achieved a marginally higher bending strength (67.7 ± 13.3 MPa) but an insulation resistance of only 70,700 MΩ, less than a third of C4's. Water absorption of 0.01% confirms a microstructure with effectively closed porosity consistent with the durability required for outdoor high voltage insulator service. This value sits within the wide range reported for porcelain insulator bodies elsewhere — spanning from around 30 MPa in vermiculite-modified indigenous-mineral formulations (Ngayakamo & Park, 2019), up to over 200 MPa where alumina and corundum content is deliberately maximized (Yousaf *et al.,* 2022)— indicating that further compositional refinement, such as the partial alumina/silica substitution explored by *Mehta et al.,* (2018), could offer a route to bending strengths beyond the 65 MPa minimum achieved here. Batch C1 at 1200 °C also satisfied both individual standards, but by a substantially narrower margin on insulation resistance, which is the basis for identifying C4 as the preferred formulation overall.

These results have direct implications for Tanzania’s ceramic industry and electricity infrastructure. Tanzania's generation capacity of 1,564 MW in 2013 is projected to reach 48,000 GWh by 2035 (Ministry of Energy and Minerals, 2013), driving proportional growth in insulator demand that is currently met entirely through importation. The present study establishes that the three principal raw materials required are available domestically, and that their combination at the identified optimum proportions and firing temperature produces a fired product meeting international specification. This provides the technical foundation for feasibility assessment of domestic high voltage ceramic insulator production, with potential to reduce import dependency, add value to local mineral resources, and strengthen the national electricity infrastructure supply chain.

5.0 Conclusion

This study has established that locally sourced Tanzanian ceramic minerals, Pugu kaolin, KIDT quartz, and Kilimanjaro feldspar, are technically suitable for the production of high voltage porcelain insulators meeting international performance standards. The principal conclusions are:

(i) The optimum formulation is Batch C4: 33 wt.% Pugu kaolin, 11 wt.% KIDT quartz, and 56 wt.% Kilimanjaro feldspar, fired at a maximum temperature of 1200 °C. This combination yields an insulation resistance of 205,800 MΩ at 1000 V DC, a bending strength of 65.358 MPa, and a water absorption of 0.01%, all meeting or substantially exceeding the minimum international standards.

(ii) Among the three firing temperatures investigated, 1200 °C is optimal. Under-firing at 1100 °C leaves residual open porosity that impairs both dielectric and mechanical performance. Over-firing at 1300 °C induces bloating porosity and micro-cracking from the quartz-to-cristobalite phase transformation, reducing properties below the 1200 °C peak.

(iii) XRD confirmed that firing Pugu kaolin generates mullite ($3Al_2O_3{\cdot}2SiO_2$), a reinforcing phase whose needle-like crystallite morphology strengthens the ceramic matrix and contributes to the high measured insulation resistance. Feldspar dissolution generates the glassy matrix that densifies the body, while quartz provides dimensional stability through the green and early-firing stages.

(iv) Increasing kaolin content beyond 48 wt.% while reducing feldspar progressively degrades both insulation resistance and bending strength across all firing temperatures, establishing clear compositional boundaries for compliant formulation design.

These findings provide a technically sound basis for advancing domestic ceramic insulator production in Tanzania to the high voltage grade, a product class currently met entirely through importation, and for leveraging the country's mineral endowment more fully in support of its growing electricity infrastructure.

6.0 Recommendations

The following recommendations arise from this work:

Pilot-scale fabrication trials should be conducted using the optimum C4 formulation at 1200 °C in industrial kilns and with mould geometries representative of actual high voltage insulator profiles (disc, pin, or long-rod types), to validate laboratory findings and identify processing challenges not apparent at specimen scale.

Scanning electron microscopy (SEM) with energy-dispersive X-ray spectroscopy (EDS) should be applied to characterize the microstructure of optimum specimens directly, enabling quantitative measurement of mullite crystallite morphology, glassy phase distribution, and residual pore geometry.

The full suite of IEC standard tests for ceramic insulators, including dielectric breakdown voltage, impulse withstand voltage, thermal shock resistance, and pollution flashover, should be conducted on pilot-scale specimens to confirm compliance across all high voltage service requirements.

A techno-economic feasibility analysis comparing the production cost of locally manufactured high voltage ceramic insulators with the import cost of equivalent products would provide the commercial justification required to attract investment in scale-up manufacturing capacity.

7.0 Funding Statement

This study was financially supported by Commission for Science and Technology (COSTEC).

8.0 Acknowledgments

We would like to acknowledge the management and staff of the Kilimanjaro Industrial Development Trust (KIDT) for their material contributions and support during data collection, and to the Korean Institute of Ceramic Engineering and Technology (KICET) for providing access to analytical laboratory equipment.

9.0 Declaration of Conflicting Interests

The authors declare no conflict of interest.

10.0 References

Conte, S., Molinari, C., Ardit, M., Cruciani, G., & Dondi, M. (2023). Porcelain versus porcelain stoneware: So close, so different—Sintering kinetics, phase evolution, and vitrification paths. *Materials*, *16*(1), 171. https://doi.org/10.3390/ma16010171

Correia, S. L., Oliveira, A. P. N., Hotza, D., & Segadães, A. M. (2006). Properties of triaxial porcelain bodies: Interpretation of statistical modeling. *Journal of the American Ceramic Society*, *89*(11), 3356-3365. https://doi.org/10.1111/j.1551-2916.2006.01245.x

Ekpunobi, U., Ihueze, C. C., Igbokwe, P., Ekpunobi, A., Obiora-Ilouno, H., Onu, C., Agbo, S., Ezennaya, S., Onuigbo, U., Tabugbo, I., Etukudoh, A., Onu, C., & Amalu, E. (2021). Production of electrical porcelain insulators from local raw materials: A review. In G. M. D. Nascimento (Ed.), *Clay and Clay Minerals*. Intech Open. https://doi.org/10.5772/intechopen.98902

IEC 60038. (2022). *IEC 60038:2009+AMD1:2021 CSV -IEC Standard Voltages*. https://webstore.iec.ch/publication/74467

IEC 60305. (2020). *IEC 60305:1995+AMD1:2020 CSV — Insulators for Overhead Lines with a Nominal Voltage Above 1000 V.* https://webstore.iec.ch/publication/1257

Kasrani, S., Harabi, A., Barama, S.-E., Foughali, L., Benhassine, M.-T., & Aldhayan, D. M. (2016). Sintering and dielectric properties of a technical porcelain prepared from economical natural raw materials. *Cerâmica*, *62*(364), 405–412. https://doi.org/10.1590/0366-69132016623641994

Kasrani, S., Harabi, A., Benhassine, M.-T., Foughali, L., & Aldhayan, D. M. (2024). Effect of Al_2O_3 additions on the dielectric properties of a porcelain insulator prepared from economical natural raw materials. *Ceramics-Silikáty*, *68*(1), 1–6. https://doi.org/10.13168/cs.2023.0052

Liu, Q., Gao, J., Liu, X., & Du, H. (2021). Phase formation, microstructure development, and mechanical properties of kaolin-based mullite ceramic added with Fe2O3. *International Journal of Applied Ceramic Technology*, *18*(3), 724–735. https://doi.org/10.1111/ijac.13720

Martín-Márquez, J., Rincón, J. M., & Romero, M. (2010). Mullite development on firing in porcelain stoneware bodies. *Journal of the European Ceramic Society*, *30*(7), 1419-1430. https://doi.org/10.1016/j.jeurceramsoc.2009.09.018

Mehta, N. S., Sahu, P. K., Tripathi, P., Pyare, R., & Majhi, M. R. (2018). Influence of alumina and silica addition on the physico-mechanical and dielectric behavior of ceramic porcelain insulator at high sintering temperature. *Boletín de La Sociedad Española de Cerámica y Vidrio*, *57*(4), 151-159. https://doi.org/10.1016/j.bsecv.2017.11.002

Merga, A., Murthy, H. N., & Aga, M. M. (2019). Fabrication of electrical porcelain insulator from ceramic raw materials of Oromia region, Ethiopia. *Heliyon*, *5*(9), e02327. https://doi.org/10.1016/j.heliyon.2019.e02327

Ministry of Energy and Minerals. (2013). *National Energy Policy Review and Generation Capacity Report (April 2013)*. Ministry of Energy and Minerals.

Mziray, S. P., Hellar-Kihampa, H., Lugwisha, E. J., & Akwilapo, L. D. (2022). Mineralogical and physicomechanical characterization of kaolinitic clay from Moshi, northern Tanzania for potential ceramic utilization. *Tanzania Journal of Science*, *48*(4), 942–953. https://doi.org/10.4314/tjs.v48i4.19

National Electrical Testing Association (NETA). (2007). *Acceptance Testing Specifications for Electrical Power Equipment and Systems (ATS-2007)*. International Electrical Testing Association.

Ngayakamo, B., & Park, E. (2019). Evaluation of Kalalani vermiculite for production of high strength porcelain insulators. *Science of Sintering*, *51*(2), 223–232. https://doi.org/10.2298/SOS1902223N

Ngayakamo, B., & Park, S.-E. (2018). Evaluation of Tanzania local ceramic raw materials for high voltage porcelain insulators production. *Cerâmica*, *64*(372), 570–576. https://doi.org/10.1590/0366-69132018643722427

Philip, K. A., Jammeh, K., & Odour, J. (2022). *An Outlook of Energy Demand, Supply and Cost in Tanzania* (Working Paper No. 370). African Development Bank.

Sadli, A., Harabi, A., Benhassine, M.-T., Foughali, L., & Kasrani, S. (2024). Investigations on kaolin mixtures: Impact on mullite formation kinetics and microstructure evolution. *International Journal of Applied Ceramic Technology*, *21*(6), 3904–3916. https://doi.org/10.1111/ijac.14742

Sánchez, E., García-Ten, J., Sanz, V., & Moreno, A. (2010). Porcelain tile: Almost 30 years of steady scientific-technological evolution. *Ceramics International*, *36*(3), 831–845. https://doi.org/10.1016/j.ceramint.2009.11.016

SEAMIC. (2008). *Mining and Mineral Resources in East and Southern Africa: An Investment Guide*. SEAMIC.

TANESCO/EWURA. (2023). *Electricity Sub-Sector Regulatory Performance Report for Financial Year 2021–2022*. Energy and Water Utilities Regulatory Authority (EWURA). https://www.ewura.go.tz

Yousaf, M., Iqbal, T., Hussain, M. A., Tabish, A. N., Haq, E. U., Siddiqi, M. H., Yasin, S., & Mahmood, H. (2022). Microstructural and mechanical characterization of high strength porcelain insulators for power transmission and distribution applications. *Ceramics International*, *48*(2), 1603-1610. https://doi.org/10.1016/j.ceramint.2021.09.239

Zanelli, C., Raimondo, M., Guarini, G., & Dondi, M. (2022). Porcelain stoneware: A critical review of 45 years of research and innovation. *Journal of the European Ceramic Society*, *42*(3), 545–572. https://doi.org/10.1016/j.jeurceramsoc.2021.10.024